Anal. Chem. **2008,** *80,* 2780−2788

Imaging MALDI Mass Spectrometry Using an Oscillating Capillary Nebulizer Matrix Coating System and Its Application to Analysis of Lipids in Brain from a Mouse Model of Tay−Sachs/Sandhoff Disease

Yanfeng Chen,[†] Jeremy Allegood,[†] Ying Liu,[‡] Elaine Wang,[‡] Begoña Cachón-González,[§] Timothy M. Cox,[§] Alfred H. Merrill, Jr.,[†,‡] and M. Cameron Sullards*[,†,‡]

Schools of Chemistry and Biochemistry and Biology, The Parker H. Petit Institute for Bioengineering and Bioscience, 315 Ferst Drive, Georgia Institute of Technology, Atlanta, Georgia 30332-0363, and Department of Medicine, University of Cambridge, Level 5, BOX 157, Addenbrooke's Hospital, Hills Road, Cambridge CB2QQ, United Kingdom

The quality of tissue imaging by matrix-assisted laser desorption/ionization mass spectrometry (MALDI-MS) depends on the effectiveness of the matrix deposition, especially for lipids that may dissolve in the solvent used for the matrix application. This article describes the use of an oscillating capillary nebulizer (OCN) to spray small droplets of matrix aerosol onto the sample surface for improved matrix homogeneity, reduced crystal size, and controlled solvent effects. This system was then applied to the analysis of histological slices of brains from mice with homozygous disruption of the hexb gene ($hexb^{-/-}$), a model of Tay−Sachs and Sandhoff disease, versus the functionally normal heterozygote ($hexb^{+/-}$) by imaging MALDI-MS. This allowed profiling and localization of many different lipid species, and of particular interest, ganglioside GM2, asialo-GM2 (GA2), and sulfatides (ST). The presence of these compounds was confirmed by analysis of brain extracts using electrospray ionization in conjunction with tandem mass spectrometry (MS/MS). The major fatty acid of the ceramide backbone of both GM2 and GA2 was identified as stearic acid (18:0) versus nervonic acid (24:1) for ST by both tissue-imaging MS and ESI-MS/MS. GM2 and GA2 were highly elevated in $hexb^{-/-}$ and were both localized in the granular cell region of the cerebellum. ST, however, was localized mainly in myelinated fiber (white matter) region of the cerebellum as well as in the brain stem with a relatively uniform distribution and had similar relative signal intensity for both $hexb^{+/-}$ and $hexb^{-/-}$ brain. It was also observed that there were distinct localizations for numerous other lipid subclasses; hence, imaging MALDI-MS could be used for "lipidomic" studies. These results illustrate the usefulness of tissue-imaging MALDI-MS with matrix deposition by OCN for histologic comparison of lipids in tissues such as brains from this mouse model of Tay−Sachs and Sandhoff disease.

Imaging matrix-assisted laser desorption/ionization mass spectrometry (MALDI-MS) is a powerful tool that can be used to determine the spatial distribution and relative abundance of specific molecules in biological samples such as histological slices of tissues.[1−4] In this technique, a MALDI matrix compound is uniformly deposited over the surface of a frozen tissue section mounted on a MALDI plate, then a pulsed laser is used to desorb and ionize compounds from specific locations (pixels) on the sample surface. The resulting ions can be separated and analyzed by MS to provide a full mass spectrum from each location. By rastering the laser across the sample surface in an ordered array, virtual images of the location of selected ions of interest may be generated. Thus, imaging MALDI-MS can be used to visualize the distribution and relative abundances of large numbers of biomolecules.

Matrix deposition is one of the factors that governs the desorption/ionization process and, thus, the quality of MALDI image in terms of mass resolution, detection sensitivity, spatial resolution, and reproducibility. The effectiveness of the matrix is determined by the size, density, analyte extraction, and homogeneity of the clusters/crystals that form on the surface. The extent to which deposition of the matrix perturbs the localization of molecules in the sample, such as the lateral diffusion of lipids that dissolve in the solvent used for matrix deposition, is also a critical factor.

Matrix deposition in imaging MALDI-MS is currently achieved by two major methods: spotting and spraying. The spotting techniques minimize the size of the spotting droplet through use

* To whom correspondence should be addressed. E-mail: cameron.sullards@chemistry.gatech.edu.

[†] School of Chemistry and Biochemistry, Georgia Institute of Technology.

[‡] School of Biology, Georgia Institute of Technology.

[§] University of Cambridge.

(1) Caprioli, R. M.; Farmer, T. B.; Gile, J. *Anal. Chem.* **1997**, *69*, 4751.

(2) Chaurand, P.; Schwartz, S. A.; Caprioli, R. M. *Anal. Chem.* **2004**, *76*, 86A.

(3) Rubakhin, S. S.; Greenough, W. T.; Sweedler, J. V. *Anal. Chem.* **2003**, *75*, 5374.

(4) McDonnell, L. A.; Heeren, R. M. A. *Mass Spectrom. Rev.* **2007**, *26*, 606.

10.1021/ac702350g CCC: $40.75
Published on Web 03/04/2008

of microspotting techniques[5–7] and have been integrated into commercially available imaging MALDI-MS systems. However, spotting can produce nonuniform distribution of matrix crystals and matrix–analyte partitioning,[8–10] and the spots are typically tens of micrometers and larger,[5–7] which is near the limit of the imaging resolution using irregular laser beams[11] and too large for better focused laser beams that can achieve higher resolution.[12–14] Application of the matrix by spraying has the advantage that the sample surface is coated more homogeneously (hence, has been used widely in imaging MALDI-MS applications).[15,16] However, the currently used techniques also have a number of technical limitations. For examples, most airbrush spraying techniques[5] have poor reproducibility because they are performed manually, and electrospray deposition, while providing more monodisperse droplets and smaller matrix crystals,[1,17] is limited in the types of solvents and matrix concentrations that can be used (due to capillary clogging), has longer sample preparation times due to the slower flow rates, and requires a conductive surface, which can complicate the analysis by the possibility of desorption electrospray ionization (DESI) also occurring.[18] In addition, for both of these matrix coating techniques, the solvent droplet might not only affect the nature of the matrix–analyte cocrystallization but also cause lateral diffusion of some of the analytes.

An alternative device for application of the matrix by spraying is the oscillating capillary nebulizer (OCN)[19–21] (Figure 1), which has been reported to provide a uniform matrix coating for accurate mass analysis and provides good sensitivity as well as reproducibility[22–24] but has not yet been used in imaging MS. Some of the advantages of OCN are that it is low-cost, can generate small droplets/aerosols with a narrow size distribution[20] by nebulizing the matrix solution at the capillary tip, and can effectively handle liquid compositions from 100% aqueous to 100% organic.[24] By controlling several parameters of OCN operation, the solvent content of the droplet approaching the sample surface can be manipulated[24] to reduce the analyte migration and enhance the matrix–analyte interaction. This feature demonstrates the strong potential of the OCN to improve the quality of data for imaging MALDI-MS. Furthermore, the OCN works well for both microflows (μL/min) and macroflows (mL/min) with high transport efficiencies,[19,25] which can greatly minimize the time for matrix coating. This makes the OCN matrix application system a promising sample preparation technique to accomplish automated, high-throughput, and high-quality matrix deposition for imaging mass spectrometry of biological molecules.

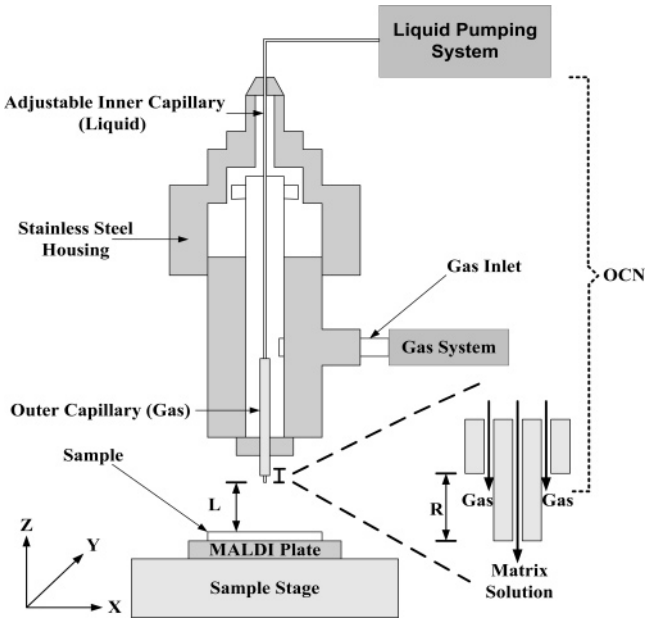

Figure 1. Schematic of the oscillating capillary nebulizer (OCN) matrix application system.

In this article, we demonstrate the use of an OCN matrix coating system coupled with imaging MALDI-MS for the analysis of lipids in tissue slices from normal brain and brain from mice with a defective hexb gene, which results in neurodegeneration due to alteration of the sphingolipid composition[26] (which we also confirm by analysis of lipid extracts using electrospray ionization tandem mass spectrometry (ESI-MS/MS) and MS^3). The studies with this mouse model for Tay–Sachs and Sandhoff disease allowed visualization of the colocation of the two elevated glycosphingolipids, GM2 and asialo-GM2 (GA2), as well as the distinct localization of other brain lipids, such as sulfatides, which do not differ noticeably between the normal and diseased brain. These results illustrate the usefulness of matrix deposition by OCN for histologic comparison of even difficult to study compounds such as lipids by tissue-imaging MALDI-MS.

EXPERIMENTAL SECTION

Chemicals. The compounds used in this study were from the following commercial sources: 2,5-dihydroxybenzoic acid (DHB) (Aldrich Chemicals, Milwaukee, WI); trifluoroacetic acid (TFA) (Fisher Scientific, Pittsburgh, PA); sulfatides (porcine brain) and

(5) Schwartz, S. A.; Reyzer, M. L.; Caprioli, R. M. *J. Mass Spectrom.* **2003**, *38*, 699.
(6) Aerni, H. R.; Cornett, D. S.; Caprioli, R. M. *Anal. Chem.* **2006**, *78*, 827.
(7) Baluya, D. L.; Garrett, T. J.; Yost, R. A. *Anal. Chem.* **2007**, *79*, 6862.
(8) Hensel, R. R.; King, R. C.; Owens, K. G. *Rapid Commun. Mass Spectrom.* **1997**, *11*, 1785.
(9) Axelsson, J.; Hoberg, A.-M.; Waterson, C.; Myatt, P.; Shield, G. L.; Varney, J.; Haddleton, D. M.; Derrick, P. J. *Rapid Commun. Mass Spectrom.* **1997**, *11*, 209.
(10) Canas, B.; Pineiro, C.; Calvo, E.; Lopez-Ferrer, D.; Gallardo, J. M. *J. Chromatogr., A* **2007**, *1153*, 235.
(11) Jurchen, J. C.; Rubakhin, S. S.; Sweedler, J. V. *J. Am. Soc. Mass Spectrom.* **2005**, *16*, 1654.
(12) Stockle, R.; Setz, P.; Deckert, V.; Lippert, T.; Wokaun, A.; Zenobi, R. *Anal. Chem.* **2001**, *73*, 1399.
(13) Spengler, B.; Hubert, M. *J. Am. Soc. Mass Spectrom.* **2002**, *13*, 735.
(14) Chaurand, P.; Schriver, K. E.; Caprioli, R. M. *J. Mass Spectrom.* **2007**, *42*, 476.
(15) Cha, S.; Yeung, E. S. *Anal. Chem.* **2007**, *79*, 2373.
(16) Garrett, T. J.; Prieto-Conaway, M. C.; Kovtoun, V.; Bui, H.; Izgarian, N.; Stafford, G.; Yost, R. A. *Int. J. Mass Spectrom.* **2007**, *260*, 166.
(17) Altelaar, A. F. M.; Van Minnen, J.; Jimenez, C. R.; Heeren, R. M. A.; Piersma, S. R. *Anal. Chem.* **2005**, *77*, 735.
(18) Wiseman, J. M.; Puolitaival, S. M.; Takats, Z.; Cooks, R. G.; Caprioli, R. M. *Angew. Chem., Int. Ed.* **2005**, *44*, 7094.
(19) Wang, L.; May, S. W.; Browner, R. F. *J. Anal. At. Spectrom.* **1996**, *11*, 1137.
(20) Reyderman, L.; Stavchansky, S. *Pharm. Dev. Technol.* **1996**, *1*, 223.
(21) Perez, J.; Petzold, C. J.; Watkins, M. A.; Vaughn, W. E.; Kenttamaa, H. I. *J. Am. Soc. Mass Spectrom.* **1999**, *10*, 1105.
(22) Lake, D. A.; Johnson, M. V.; McEwen, C. N.; Larsen, B. S. *Rapid Commun. Mass Spectrom.* **2000**, *14*, 1008.
(23) Fung, K. Y. C.; Askovic, S.; Basile, F.; Duncan, M. W. *Proteomics* **2004**, *4*, 3121.
(24) Basile, F.; Kassalainen, G. E.; Williams, S. K. R. *Anal. Chem.* **2005**, *77*, 3008.
(25) Kirlew, P. W.; Caruso, J. A. *Appl. Spectrosc.* **1998**, *52*, 770.
(26) Cachon-Gonzalez, M. B.; Wang, S. Z.; Lynch, A.; Ziegler, R.; Cheng, S. H.; Cox, T. M. *Proc. Natl. Acad. Sci. U.S.A.* **2006**, *103*, 10373.

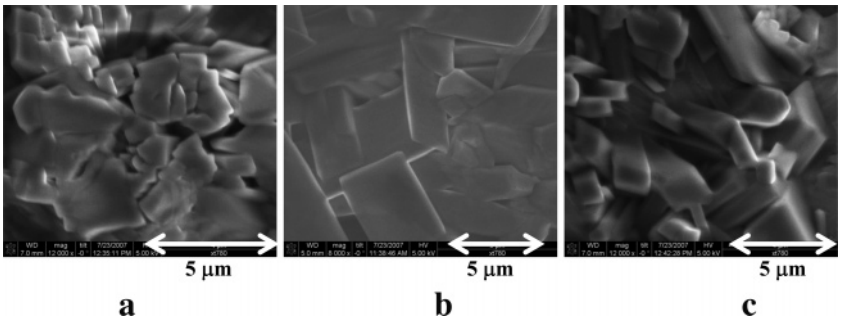

Figure 2. SEM images of DHB crystals formed using different OCN parameters of matrix solution flow rate, N_2 pressure, and sprayer−sample distance. (a) 100 μL/min, 40 psi, and 4 cm; (b) 75 μL/min, 50 psi, and 8 cm; (c) 60 μL/min, 55 psi, and 10 cm.

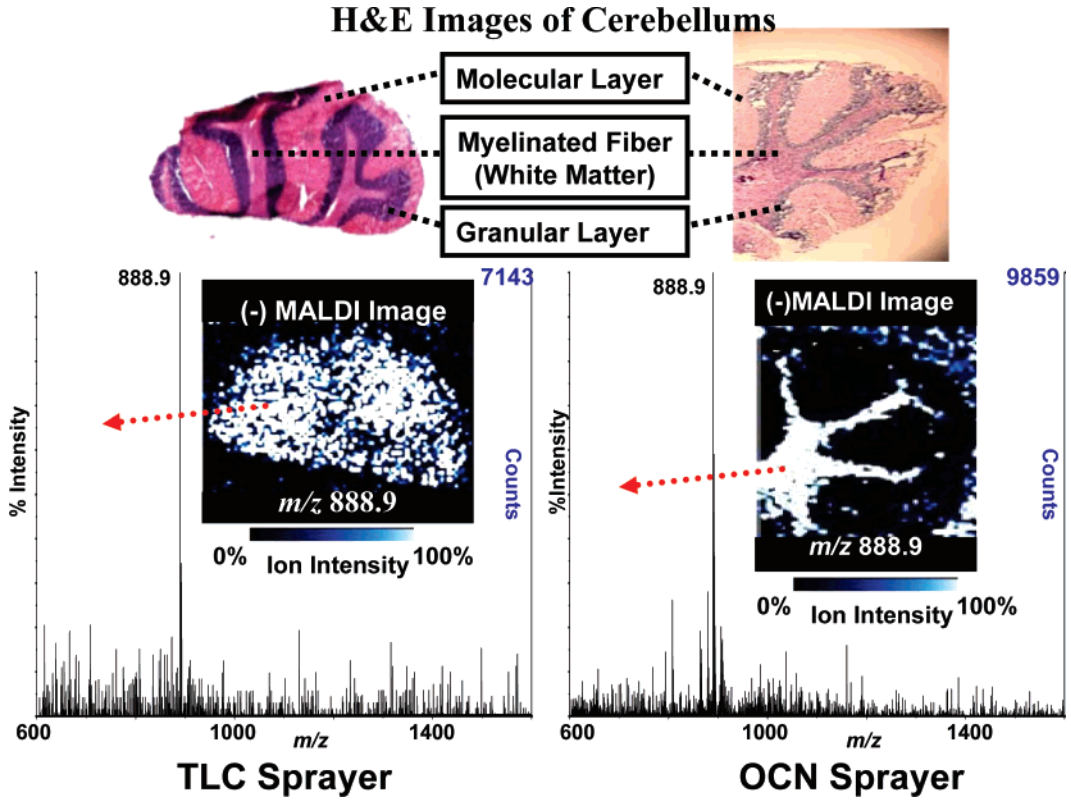

Figure 3. Representative images obtained by matrix applications using a TLC sprayer and an OCN sprayer. The fine structures (molecular layer, myelinated fiber, and granular layer) of hexb$^{+/-}$ mouse brain (cerebellum) are labeled in the upper H and E stained images. Negative ion mode MALDI images of *m/z* 888.9 found in mouse brain tissues together with MALDI mass spectra generated from specific brain spots are shown at lower left and lower right, respectively.

a total ganglioside mixture (porcine brain) (Avanti Polar Lipids Inc., Alabaster, AL); monosialogangliosides GM1, GM2, and GM3 (as NH_4^+ salts) (Matreya LLC, Pleasant Gap, PA); hematoxylin−eosin (H and E) staining solution (VWR, West Chester, PA). All solvents were HPLC grade (EMD Chemicals, Gibbstown, NJ), and Nanopure water (18 MΩ) was used throughout the experiments.

Experimental Animals. The brains from hexb$^{+/-}$ and hexb$^{-/-}$ mice (bred from strain B6;129S-Hexbtm1Rlp, Jackson Laboratory, with confirmation of the hexb genotype by PCR) were obtained as described in a previous publication.[26] The studies were conducted using protocols approved under license by the U.K. Home Office (Animals Scientific Procedures Act, 1986).

Tissue Sectioning. The dissected brains were frozen in liquid nitrogen and stored at −80 °C. Before tissue section, the frozen brains were first put into a sealed dry ice box to equilibrate at that temperature for 60 min, then they were transferred into the cryostat at −20 °C for another 60 min before sectioning as 10 μm slices at −18 °C and thaw-mounted onto chilled MALDI plates. Neighboring sections were also cut under the same conditions and thickness, then thaw-mounted onto glass slides for histological staining. The tissue slices on the MALDI plates were slowly brought to room temperature in a desiccator before matrix coating.

Histological Staining. Tissue sections on glass slides were stained using routine protocol of H and E staining for frozen sections on a Leica autostainer XL (Leica Microsystems, Bannockburn, IL). The histological images were taken with a Nikon Eclipse E600 microscope (Nikon, Melville, NY).

Optimized TLC Sprayer Conditions. The TLC conditions were optimized according to a previously published report.[5] A 25 mL TLC reagent sprayer with standard ground glass joint (Kimble/Kontes, Vineland, NJ) was used to spray matrix solution (30 mg/mL DHB in 50:50, v/v, acetonitrile/water with 0.1% TFA)

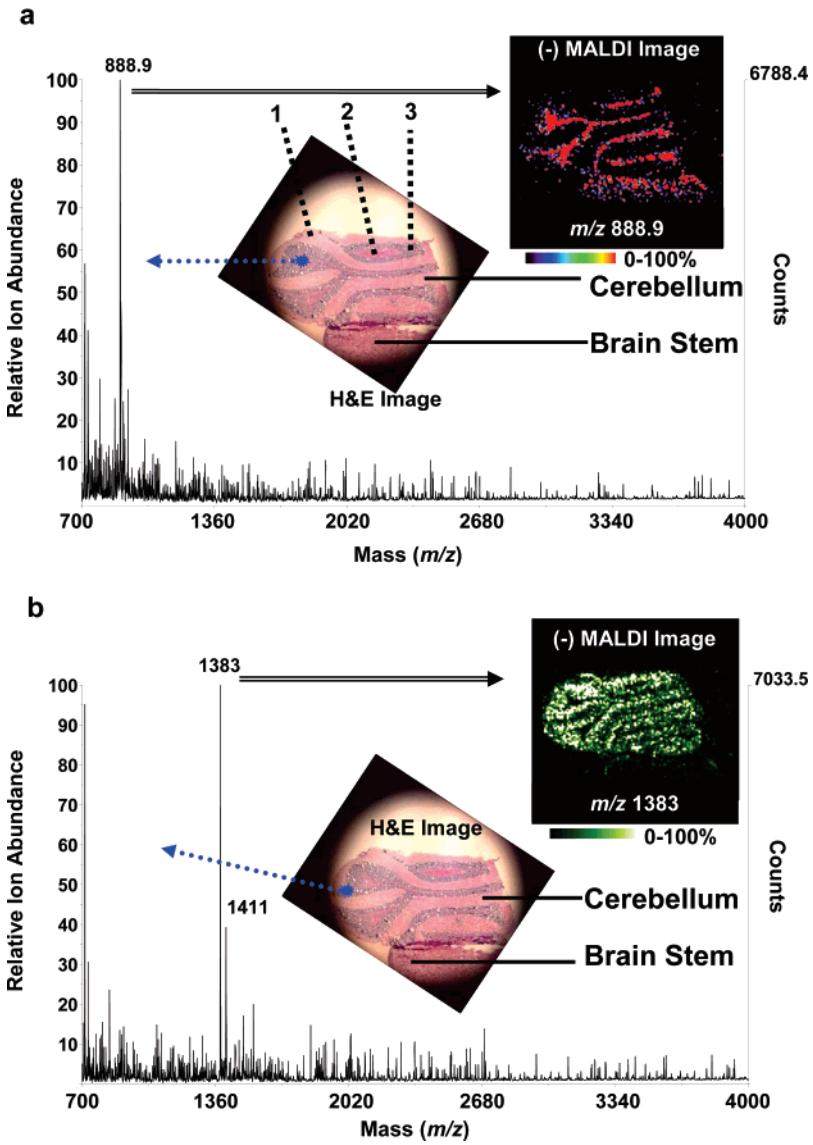

Figure 4. Imaging MALDI-MS data from hexb$^{-/-}$ mouse brain (cerebellum, 7.164 mm × 3.729 mm) using negative ion mode. The fine structures of cerebellum in the H and E stained images are labeled as (1) molecular layer, (2) myelinated fiber (white matter), and (3) granular layer. The MALDI spectra present the ion yield from specific spots in (a) myelinated fiber (white matter) and (b) granular layer region, respectively. The molecular distributions of *m*/*z* 888.9 ions and *m*/*z* 1383 ions are shown in (a) and (b), respectively.

onto the brain tissue. The operating pressure of nitrogen was ~7 psi. The distance between the nozzle and the sample was ~12 cm. Multiple matrix coating cycles with discrete spraying and drying were performed to get better imaging results. Typically, the spraying and drying time for a 10 × 10 mm^2 sample was 10 and 30 s, respectively. Usually 30 coating cycles were required for the brain tissues to provide an optimal matrix thickness of 5 to ~50 μm. The average crystal size of DHB matrix using this protocol was ~100 μm.

OCN Matrix Application System. A diagram of the design and operation of the OCN matrix application system is shown in Figure 1. The matrix solution (30 mg/mL DHB in 50:50, v/v, acetonitrile/water with 0.1% TFA) was delivered to the OCN sprayer using a syringe pump (KD Scientific, Holliston, MA) at a flow rate of ~60 μL/min. The OCN sprayer[19,21] consists of two coaxial fused-silica capillary tubes (Polymicro Technologies, LLC, Phoenix, AZ) that are friction-fit-mounted with PEEK sleeves (Upchurch Scientific, Oak Harbor, WA) housed in a $^1/_{16}$ in. stainless steel union tee (Swagelok, Solon, OH). The inner capillary (i.d. 50 μm, o.d 150 μm, length 80 mm) was used to transfer the matrix solution, and the outer capillary (i.d. 250 μm, o.d. 350 μm, length 30 mm) allowed nitrogen (~50 psi) to pass through the annular space between the outer wall of inner capillary and inner wall of the outer capillary to generate the oscillation of the inner capillary tip, which extends about 1 mm (R) from the outer capillary tip. The high-frequency oscillation induces the nebulization of the matrix solution and generates a fine and uniformly dispersed spray of matrix droplets/particles. The typical distance (L) between the OCN and the sample on the *xyz* translation stage (Newport, Irvine, CA) is ~10 cm depending on the flow rate of the matrix solution and gas pressure. The sample was continually moved across the aerosol deposition area in the *X* direction (5 mm/s) and *Y* direction (5 mm/s) to obtain an even matrix distribution throughout the sample surface. The typical time of matrix coating for a 4 cm^2 sample is about 5 min with an estimated thickness of 10−20 μm.

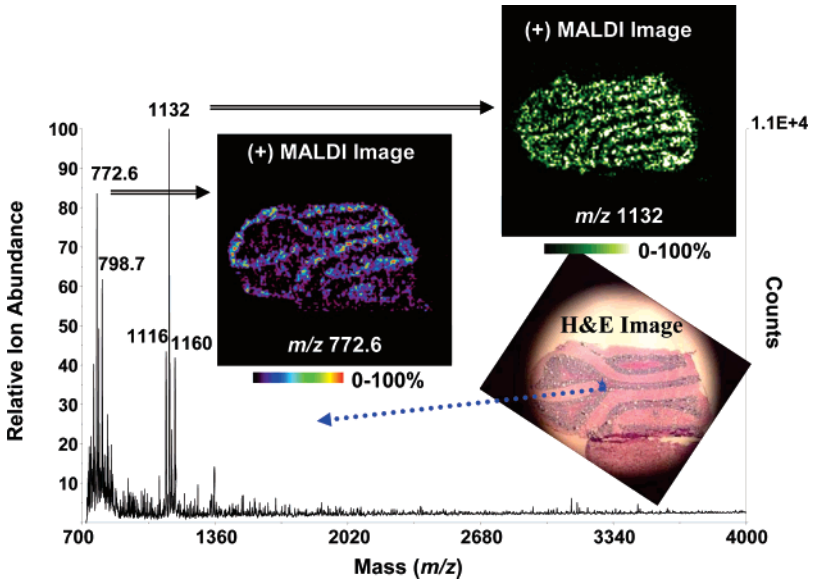

Figure 5. Imaging MALDI-MS data from hexb$^{-/-}$ mouse brain (cerebellum, 7.164 mm × 3.729 mm) using positive ion mode. The MALDI spectrum presents the ion yield from a spot at the boundary of molecular layer and granular layer regions. The molecular distributions of *m*/*z* 772.6 and *m*/*z* 1132 are compared with the H and E stained image.

Scanning Electron Microscopy. The characteristics of the applied matrix crystals using different conditions was determined using a scanning electron microscope (SEM) on a Nova Nanolab 200 system (FEI company, Hillsboro, OR). The accelerator voltage of the SEM system was typically 5 kV. No carbon or gold were further coated to the matrix surface prior to the SEM analysis.

Imaging MALDI-MS. MALDI mass spectra were acquired using a Voyager DE STR MALDI-TOF-MS (Applied Biosystems) with a 337 nm N_2 laser (3 Hz, ~100 μm) under delayed extraction conditions in reflector mode. The accelerating voltage, grid voltage, and delay time were 22 kV, 70%, and 400 ns, respectively. The mass spectrometer was calibrated using sulfatides (porcine brain) and a total ganglioside mixture (porcine brain). Imaging MALDI-MS data sets were acquired using modified MMSIT (without 32k data limitation) over the tissue section. In this work, nine shots were summed on each sample spot and the step size of sample stage was 60 μm. Ion images were reconstituted using BioMap software package (Novartis Pharma AG, Basel, Sweden).

ESI-MS^n. GM2, GA2, and sulfatide were analyzed by ESI-MS/MS and ESI-MS^3 to confirm both their identities and determine their structures. Briefly, the tissues were homogenized (10 mg/mL) in 10 mM potassium phosphate buffer (pH 7.4) on ice, extracted, and the acidic glycolipids recovered by batch elution from a DEAE column.[27] The final extracts were dissolved in 1.0 mL of MeOH and introduced via syringe infusion (0.6 mL/h) into an API 4000 QTrap tandem mass spectrometer. Acidic gangliosides and sulfatides were examined in negative ion mode, whereas neutral glycosphingolipids were examined in positive ion mode.

Sulfatides fragment via cleavage and charge retention by their sulfate to yield a primary product ion of *m*/*z* 96.9. Precursor ion scans for *m*/*z* 96.9 were used to determine the potential *N*-acyl chain length subspecies in each sample. These scans were performed with declustering potential (DP) of −220 eV and collision energies ranging from −100 to −120 eV. Once individual sulfatide subspecies were identified, ionization conditions were optimized for each and enhanced product ion (EPI) scans were performed to structurally identify the sulfatide species because it revealed a greater diversity of product ions than Q3 scans. EPI scans were performed with Q0 trapping set to "on", a linear ion trap fill time of 100 ms, and a scan rate of 1000 amu/s.

Acidic gangliosides fragment primarily via cleavage of their sialic acids (*m*/*z* 290.1) and other glycans. Precursor ion scans for *m*/*z* 290.1 were used to identify the potential *N*-acyl chain length subspecies within each family of acidic gangliosides (i.e., GM1, GD1, GT1). These scans were performed with DP of −70 to −100 eV (lower DP was required to reduce in-source fragmentation for species having multiple sialic acid residues). Collision energies ranged from −55 to −75 eV with lower collision energies used for species having increasing numbers of sialic acid residues because of the liability of these molecules toward fragmentation. Once individual ganglioside subspecies were identified, ionization conditions were optimized for each and EPI scans were performed with Q0 trapping set to "on", a linear ion trap fill time of 100 ms, and a scan rate of 1000 amu/s. An MS^3 analysis is performed in much the same manner as a product ion scan. In this case the first mass analyzer (Q1) is set to "open" to pass a wide *m*/*z* window (6−10 amu) around the precursor ion of interest, which is transmitted to Q2 where it collides with a neutral gas (N_2) and dissociates to various fragment ions. Rather than mass analyzing the resulting product ions, the linear ion trap (LIT) is set to trap and hold a 2 *m*/*z* unit window centered on the product ion of interest. The selected *m*/*z* ions are then irradiated with a single wavelength, amplitude frequency to induce further fragmentation to secondary product ions, which are then scanned out of the LIT. The sphingoid base and fatty acid composition of each ganglioside can be successfully identified by MS^3 analysis.

Neutral glycosphingolipids were analyzed in positive ion mode as both $(M + H)^+$ and $(M + Na)^+$ species. Neutral glycosphingolipids fragment primarily via cleavage of carbohydrate groups.

(27) van Echten-Deckert, G. Sphingolipid Extraction and Analysis by Thin-Layer Chromatography. In *Sphingolipid Metabolism and Cell Signaling, Part B*; Academic Press Inc.: San Diego, CA, 2000; Vol. 312, p 64.

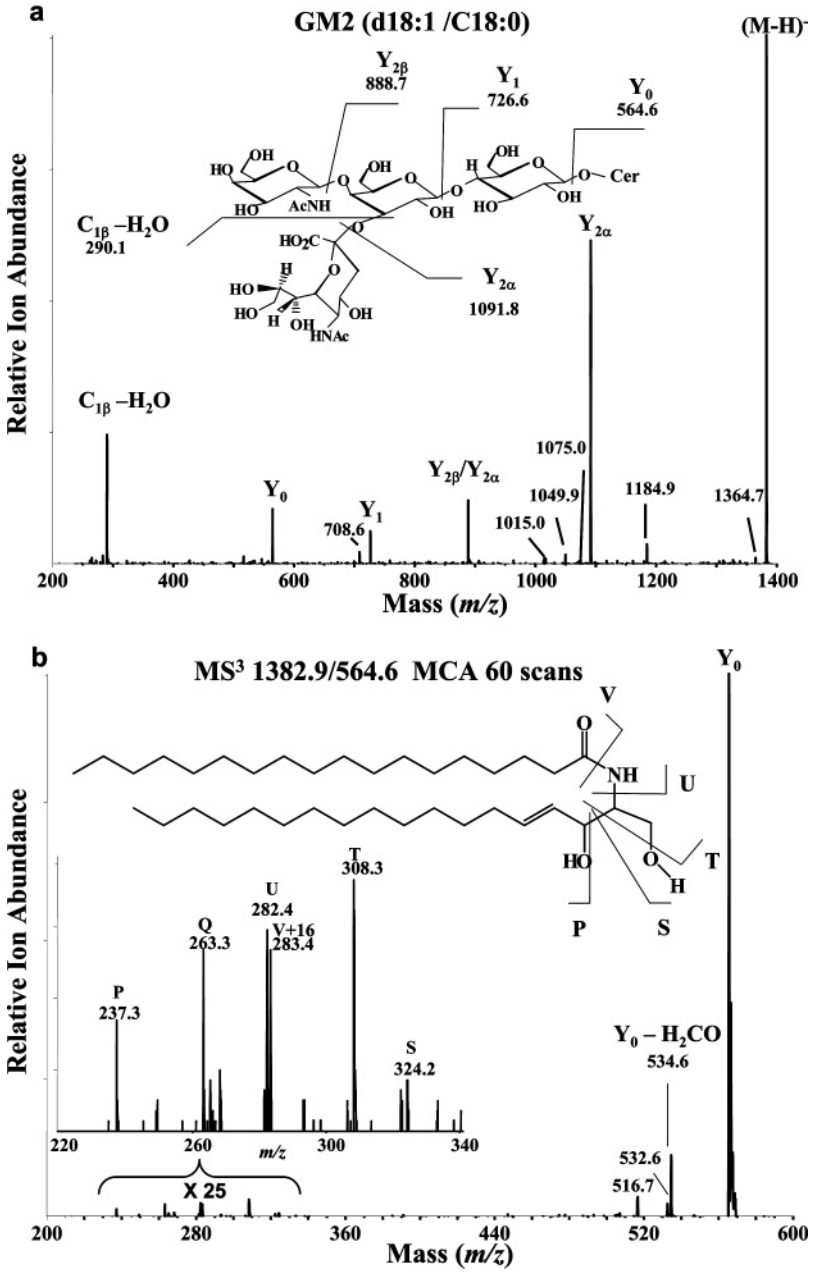

Figure 6. (a) ESI-MS/MS spectrum of *m*/*z* 1383 and (b) ESI-MS^3 spectrum of the 1383/564 transition.

Potential subspecies were identified via neutral loss scans for hexose and *N*-acetyl-hexosamine (162 and 203 u, respectively). The parameters of EPI and MS^3 scans for neutral glycosphingolipids were kept the same as those for acidic gangliosides.

RESULTS AND DISCUSSION

Use of OCN for Matrix Deposition. There are several variables required to achieve the desired coating of the sample with small and uniform matrix crystals using an OCN system. These include determination of a successful combination of matrix and solvent, flow rate of this matrix solution, pressure of the nebulizing gas, distance between sample and OCN outlet (L in Figure 1), and matrix deposition time. Other parameters that need to be considered are the inner and outer diameters of the two capillaries and the length the inner capillary tip extends from the outer capillary. These parameters have been published previously for use of this OCN for aerosol generation.[19−25]

DHB was chosen for these studies because it has been widely used for analysis of lipids and many other metabolites as well as peptides and small proteins by MALDI-MS.[28−31] DHB can be dissolved in a number of solvents, such as acetonitrile/water (50:50, v/v, with 0.1% TFA)[32] and ethanol/water (50:50, v/v, with 0.1% TFA)[5] and (90:10, v/v, with 0.1%TFA).[33] It was determined that 30 mg/mL of DHB in acetonitrile/water (50:50, v/v, with 0.1% TFA) can deposit fairly evenly distributed and small (0.5−20 μm

(28) Ng, K. M.; Liang, Z.; Lu, W.; Tang, H.-W.; Zhao, Z.; Che, C.-M.; Cheng, Y.-C. *Anal. Chem.* **2007**, *79*, 2745.
(29) Zhang, X.; Scalf, M.; Berggren, T. W.; Westphall, M. S.; Smith, L. M. *J. Am. Soc. Mass Spectrom.* **2006**, *17*, 490.
(30) Jagannadham, M. V.; Nagaraj, R. *J. Pept. Res.* **2005**, *66*, 94.
(31) Groseclose, M. R.; Andersson, M.; Hardesty, W. M.; Caprioli, R. M. *J. Mass Spectrom.* **2007**, *42*, 254.
(32) Padliya, N. D.; Wood, T. D. *Proteomics* **2004**, *4*, 466.
(33) Fujiwaki, T.; Yamaguchi, S.; Tasaka, M.; Sakura, N.; Taketomi, T. *J. Chromatogr., B: Anal. Technol. Biomed. Life Sci.* **2002**, *776*, 115.

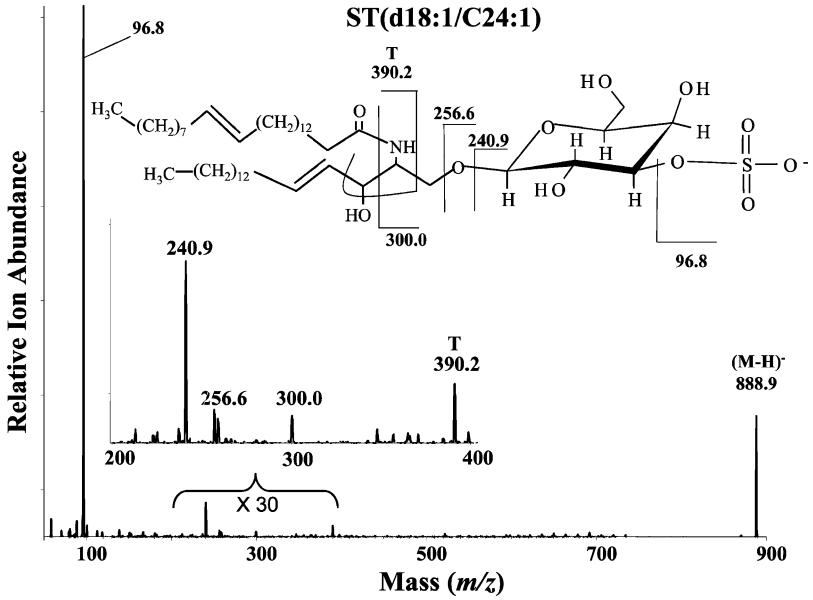

Figure 7. ESI-MS/MS of *m*/*z* 888.9.

mean diameter) matrix crystals on the tissue surface. Several different combinations of matrix solution flow rate, nebulizing gas pressure, and OCN−sample distance were evaluated for matrix deposition. The matrix molecules formed irregular clusters without obvious crystal boundaries (Figure 2a) when using a high flow rate (100 μL/min) with a low gas pressure (40 psi) and short sprayer−sample distance (4 cm). This was anticipated because these conditions would likely produce large droplets with a high solvent content.[24] A reduction of the matrix solution flow rate to 75 μL/min, while increasing both the gas pressure (50 psi) and sprayer−sample distance (8 cm), resulted in the matrix crystals becoming flat and rectangular in shape (2−5 μm in length) (Figure 2b). This presumably occurs because the droplets are smaller and the solvent has longer to evaporate and begin to form DHB crystals in flight. At an even slower flow rate (60 μL/min), and higher gas pressure (55 psi) and sprayer−sample distance (10 cm), the smallest needle-like matrix crystals (approximately 0.5 to 3 μm in length) were observed on the surface (Figure 2c). This longer sprayer−sample distance (10 cm) was selected to produce dryer DHB particles, since it has been reported that application of dry matrix compound to tissues is effective for visualization of lipids using MALDI-MS by minimizing the analyte migration induced by the solvent and yielding much greater signal response.[34]

It was determined that movement of the sample in the *X* direction (5 mm/s) and *Y* direction (5 mm/s) for the entire period of matrix deposition facilitated the formation of an even matrix layer and improved the reproducibility of sample preparation. Additionally, it was observed that a matrix thickness of between 5 and 50 μm was sufficient for reasonable signal-to-noise ratio (S/N) of lipid ions in mouse brain tissue (see below).

Examination of Mouse Brain Sphingolipids Using the OCN for Matrix Deposition. Mouse brain tissue (hexb$^{+/-}$) samples having matrix deposition by a TLC sprayer was compared to those prepared with the OCN system. The resulting MALDI-MS data revealed the formation of an ion of *m*/*z* 888.9 in both samples. This ion is subsequently shown to be a sulfatide (galactosylceramide-3-O-sulfate with the d18:1/C24:1 backbone), consistent with previous reports.[35] The MALDI-MS image of this ion in the TLC-prepared sample (Figure 3, lower left) followed the general contour of the tissue (Figure 3, upper left). However, there were no features in the image that could be unambiguously correlated with specific regions of the brain. In contrast, the MALDI-MS image of *m*/*z* 888.9 in the tissue slice with matrix deposition via the OCN (Figure 3, lower right) showed a good correlation with the H and E stained histological image (Figure 3, upper right) with regard not only to sample shape but also to the fine tissue structures. The myelinated fiber (white matter) regions in the cerebellum were all successfully illustrated by the ion image. The imaging differences between the two matrix coating techniques were highly reproducible as evidenced by multiple experiments.

These images clearly demonstrate the OCN system is useful for sample preparation for MALDI-MS imaging of lipids. An important feature of the OCN system is the ability to minimize the amount of solvent that comes into contact with the tissue. This serves to reduce analyte migration and matrix crystal size to minimize the loss of molecular spatial information. Further applications of the OCN coating system may include computer control providing more precise and reproducible matrix deposition. Additionally, this may allow multiple samples to be prepared in an unattended fashion for high-throughput sample preparation under optimal conditions.

Additional Features Noted upon MALDI-MS Imaging of Sphingolipid Subspecies in Mouse Brain. MALDI-MS spectra acquired in the negative mode for the hexb$^{-/-}$ mouse brain slices prepared by OCN matrix coating system showed two prominent ions of *m*/*z* 888.9 and 1383 (Figure 4, parts a and b) localized in different regions of the brain. The image generated from the spatial distribution of the *m*/*z* 888.9 ion (d18:1/C24:1

(34) Hankin, J. A.; Barkley, R. M.; Murphy, R. C. *J. Am. Soc. Mass Spectrom.* **2007**, *18*, 1646.

(35) Colsch, B.; Afonso, C.; Popa, I.; Portoukalian, J.; Fournier, F.; Tabet, J.-C.; Baumann, N. *J. Lipid Res.* **2004**, *45*, 281.

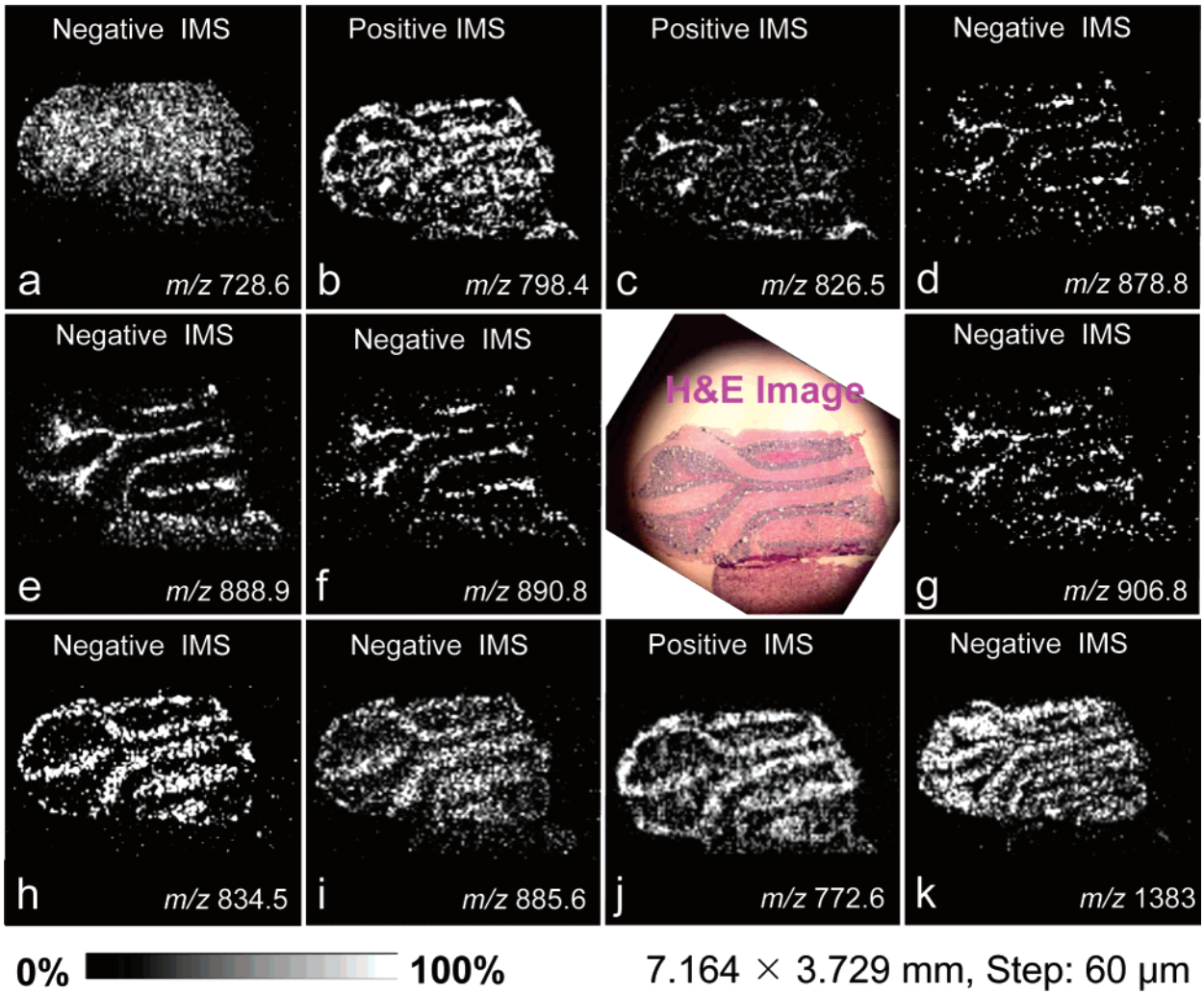

Figure 8. Selected ion images of various species from hexb$^{-/-}$ mouse brain, which illustrate different histological localizations. (a) *m*/*z* 728.6 [PlsEtn 36:1*]; (b) *m*/*z* 798.4 [PC 34:1* + K]; (c) *m*/*z* 826.5 [PC 36:1* + K]; (d) *m*/*z* 878.8 [ST(OH) d18:1/h22:0]; (e) *m*/*z* 888.9 [ST d18:1/C24:1]; (f) *m*/*z* 890.8 [ST d18:1/C24:0]; (g) *m*/*z* 906.8 [ST(OH) d18:1/h24:1]; (h) *m*/*z* 834.5 [PS 40:6*]; (i) *m*/*z* 885.6 [PI 38:4*]; (j) *m*/*z* 772.6 [PC 32:0* + K]; (k) *m*/*z* 1383 [GM2 d18:1/C18:0]. A * indicates a tentative assignment (refs 39 and 40). PC, phosphatidylcholine; PI, phosphatidylinositol; PlsEtn, plasmenylethanolamine; PS, phosphatidylserine.

sulfatide) displayed a remarkably similar pattern to the myelinated fiber (white matter) region of the cerebellum and a relatively even distribution in brain stem (cf., H and E staining) (Figure 4a). The image generated from the *m*/*z* 1383 ion (d18:1/C18:0 ganglioside GM2) most closely matched the granular cell region in cerebellum and produced no detectable ions in the brain stem region (Figure 4b).

In positive mode, a number of intense ions were seen in the range of *m*/*z* 700−1400 (Figure 5). Of particular interest are *m*/*z* 772.6 and 1132, which have significantly different localizations from each other. The ion of *m*/*z* 772.6 is found primarily in the molecular layer region, and the ion of *m*/*z* 1132 is found mainly in the granular cell region. Furthermore, it is also observed that there is a remarkable similarity in the localization of *m*/*z* 1132 (Figure 5, upper right) and *m*/*z* 1383 (Figure 4b). This is interesting because *m*/*z* 1132 corresponds to the mass of potassiated asialo-GM2(d18:1/C18:0), which is also known to accumulate in mice with this genetic defect,[36] but to our knowledge, this is the first study to visualize their colocalization.

(36) Conzelmann, E.; Sandhoff, K. *Proc. Natl. Acad. Sci. U.S.A.* **1978**, *75*, 3979.

Neither GM2 nor GA2 were detected in hexb$^{+/-}$ brains, but they were highly elevated in hexb$^{-/-}$ brains. This was in contrast to ST, which had similar signal intensities in both hexb$^{+/-}$ and hexb$^{-/-}$ brains (similar observations were also seen in the ESI-MS/MS spectra for the brain extracts, data not shown). In addition, GM2 and GA2 were observed to be colocalized in the granular layer region of cerebellum (Figures 4 and 5), whereas ST was mainly detected in the myelinated fiber (white matter) region of the cerebellum and the brain stem with a relatively uniform distribution (Figures 3 and 4).

The mass spectra and resulting ion images were obtained with only nine laser shots per spot in either the positive or negative ionization mode. This clearly demonstrates that samples that have been prepared using the OCN for matrix deposition are able to yield usable ion signals with few laser shots. These results suggest that the OCN matrix deposition system generates a good matrix−analyte interaction, which promotes efficient laser desorption and subsequent ionization of lipids. An additional benefit of the OCN system would be the ability to yield mass spectra with high S/N ions via fewer laser shots to reduce the analysis time.

Confirmation of the Identity and Structure of GM2 and Sulfatide by MS^n. Analysis of the lipid extracts from the mouse brains was performed to confirm the presence of sulfatide, GM2, and GA2 (spectra not shown). In negative ion mode, MS/MS of *m/z* 1382.9 generates five major fragment ions corresponding to losses of different sugar moieties in the head group (Figure 6a). The product ions of *m/z* 1091.8, 888.7, 726.6, and 564.6 correspond to the Y-type glycosidic bond cleavage involving loss of NeuAc, NeuAc/GalNac, NeuAc/GalNac/Gal, and NeuAc/GalNac/Gal/Glc, respectively. The *m/z* 290.1 ions were produced by C-type cleavage and charge retention on the sialic acid with subsequent dehydration, which confirms the existence of a sialic acid moiety. An MS^3 experiment was performed on the Y_0 fragment ion of *m/z* 564.6 to establish the nature of the ceramide backbone of the *m/z* 1382.9 ion. The resulting MS^3 spectra (Figure 6b) showed secondary fragment ions of *m/z* 324, 308, 282, and 283, corresponding to S, T, U, and V + 16 fragments, respectively,[37] revealing that the amide-linked fatty acid is stearate (C18:0). The ions of *m/z* 237 and 263 correspond to complimentary P and Q fragments, respectively,[37] showing that the sphingoid base backbone is d18:1. Thus, this major species in $hexb^{-/-}$ mouse brain is ganglioside GM2 (d18:1/C18:0).

MS/MS of *m/z* 888.9 in the negative ion mode (Figure 7) revealed a highly abundant fragment ion at *m/z* 96.8 corresponding to a sulfate group (HSO_4); lower abundance fragments of *m/z* 256.6 and 240.9 arise from cleavage on either side of the 1′ oxygen of the sphingoid base with charge retention on the sulfated carbohydrate. The ion of *m/z* 390.2 corresponds to a "T-type" cleavage of both of the sphingoid base and the sugar head group with charge retention on the fatty acid, which is identified as nervonic acid (C24:1). Therefore, *m/z* 888.9 can be identified as a sulfatide (galactosylceramide-3-O-sulfate) with a d18:1/C24:1 backbone configuration.

Examples of Lipids with Distinct Spatial Distributions. Several other prominent ions were distinctly visible in brain samples prepared using OCN for matrix deposition (Figure 8). Although they have not been all independently identified structurally via MS/MS, their nominal *m/z* values are consistent with previously published work.[38−40] The ions of *m/z* 728.6 (plasmenylethanolamine, PlsEtn, with C36:1*) were relatively evenly distributed throughout the cerebellum (Figure 8a), whereas *m/z* 798.4 (phosphatidylcholine, PC, with C34:1* + K) was predominantly observed in myelinated fiber (white matter) and molecular layer regions (Figure 8b). PC with C36:1* + K (*m/z* 826.5) (Figure 8c) was more specifically localized in myelinated fiber (white matter) regions, as were sulfatides, ST, with the d18:1/C24:1 and d18:1/C24:0 backbones (*m/z* 888.9 and 890.8, respectively), and hydroxylated sulfatide, ST(OH), with d18:1/h22:0 and d18:1/h24:1 ceramide backbones (*m/z* 878.8 and 906.8, respectively) (Figure 8d−g). In contrast, the ions of *m/z* 834.5 (phosphatidylserine, PS, with C40:6*), *m/z* 885.6 (phosphatidylinositol, PI, with C38:4*), and *m/z* 772.6 (PC with C32:0* + K) were highly localized in molecular layer region (Figure 8h−j, respectively), while the ion of *m/z* 1383 (ganglioside GM2 with d18:1/C18:0) was mainly distributed in granular layer region (Figure 8k). These imaging MALDI-MS results illustrate that many subcategories of lipids are localized to specific regions of the brain. Therefore, this technology is a valuable complement to other types of "lipidomic" analysis, which use homogenized extracts of the entire tissue which may miss potentially important regional changes in both the types and amounts of the present lipids.

CONCLUSIONS

This study has shown that an OCN can be used to generate good matrix homogeneity and spatial resolution for visualization of several types of lipids including sulfatides, gangliosides, and phosphoglycerolipids. The success of this method is likely due to its fine control of the amount of solvent in the droplets as they are deposited onto the sample surface. Similar to certain matrix application techniques such as airbrushing, this system's ability to become automated affords the possibility of high-throughput, high-quality matrix application for routine histologic analysis. Its usefulness has been demonstrated here for the visualization of lipids in brains from a mouse model of Tay−Sachs and Sandhoff disease, and it is very likely to have broad applications in tissue-imaging MALDI-MS of other molecules as well.

ACKNOWLEDGMENT

This work is supported by NIH GM069338 (Lipid MAPS) and seed funding from Georgia Institute of Technology for the Mass Spectrometry Bio-Imaging Center. We thank Drs. Richard Brownner and Facundo Fernandez for providing the OCN sprayer, Dr. Markus Stoeckli for sharing the modified MMIST software, Lan Sun for the SEM analysis, and Dr. Robert C. Murphy and Dr. Joseph A. Hankin for helpful discussions.

Received for review November 15, 2007. Accepted January 24, 2008.

AC702350G

(37) Merrill, A. H.; Sullards, M. C.; Allegood, J. C.; Kelly, S.; Wang, E. *Methods* **2005**, *36*, 207.
(38) Benjamins, J. A.; Hajra, A. K.; Agranoff, B. W. *Basic Neurochemistry*, 7th ed.; Elsevier Academic Press: Burlington, MA, 2006.
(39) Dreisewerd, K.; Lemaire, R.; Pohlentz, G.; Salzet, M.; Wisztorski, M.; Berkenkamp, S.; Fournier, I. *Anal. Chem.* **2007**, *79*, 2463.
(40) Jackson, S. N.; Wang, H. Y. J.; Woods, A. S. *J. Am. Soc. Mass Spectrom.* **2007**, *18*, 17.